CHINESE OPTICS LETTERS

Vol. 20, No. 1 | January 2022

Broadband achromatic polarization insensitive metalens over 950 nm bandwidth in the visible and near-infrared

Peng Sun (孙 朋)[1,2], Mengdie Zhang (张梦蝶)[2], Fengliang Dong (董凤良)[2,3*], Liefeng Feng (冯列峰)[1**], and Weiguo Chu (褚卫国)[2,3***]

[1] Tianjin Key Laboratory of Low Dimensional Materials Physics and Preparing Technology, Department of Applied Physics, School of Science, Tianjin University, Tianjin 300072, China

[2] Nanofabrication Laboratory, CAS Key Laboratory for Nanophotonic Materials and Devices, CAS Center for Excellence in Nanoscience, National Center for Nanoscience and Technology, Beijing 100190, China

[3] Center of Materials Science and Optoelectronics Engineering, University of Chinese Academy of Sciences, Beijing 100049, China

*Corresponding author: dongfl@nanoctr.cn

**Corresponding author: fengliefeng@tju.edu.cn

***Corresponding author: wgchu@nanoctr.cn

Received May 31, 2021 | Accepted July 7, 2021 | Posted Online September 27, 2021

Metalenses are expected to play an increasingly important role in miniaturized and integrated optical imaging components/systems. However, devising broadband achromatic metalenses with high focusing efficiencies is still quite challenging. In this work, we proposed an aperture-shared partition phase cooperative manipulation approach for designing a high-efficiency broadband achromatic metalens composed of two concentric sub-metalenses. As a proof-of-concept, an achromatic polarization-independent metalens is successfully designed for the visible and near-infrared range from 450 nm to 1400 nm with the focusing efficiency over 70% for the wavelength range of 600 nm to 1400 nm. The approach reported here provides a possibility for designing a high-performance metalens, which has great potential applications in integrated optics.

Keywords: achromatic metalens; efficiency; broadband; polarization independence.
DOI: 10.3788/COL202220.013601

1. Introduction

Traditional bulky and heavy optical lenses are gradually difficult to keep pace with the requirements of the rapid development of miniaturized and integrated optical components/systems. However, considering the strong and unique capability of locally manipulating the amplitude, phase, and polarization to shape the wavefront of light with subwavelength resolution, planar metalenses consisting of plasmonic or dielectric nano-scatterers may play a critical role[1–6]. In the past decade, although the reflective metalens had been studied[7–9], the metal loss introduced by using a metal film as the reflective surface resulted in low light energy utilization. Later, the principle of surface plasmon resonance (SPR)[4,10–13] was used to design transmissive metalenses[13–16]. This method increases the surface electric field strength, but the absorption loss of metal is still unavoidable. Therefore, in recent years, most metalenses were designed by all-dielectric materials[17–19], which avoid the loss, and the transmissive metalenses account for the vast majority of metalens practical applications[20–23]. Despite this, the exploration of metalenses with excellent comprehensive performance, such as the combination of chromatic aberration, broadband, and high focusing efficiency, is still far from being satisfactory.

For the transmissive metalens working at a specific wavelength regardless of the bandwidth, its efficiency can be optimized by designing the proper geometry and dimension of meta-atoms based on the materials with low enough absorptivity to reasonably impart the target phase. A good case in point is the amorphous silicon metalens designed for an operating wavelength of 1550 nm with a high measured focusing efficiency of up to 82%[24]. However, for a broadband metalens, the chromatic aberration induced by the intrinsic dispersion of the meta-atom material would give rise to different phase manipulations for different wavelengths and thus results in the change of its focus length (FL) against the working wavelength, which is unfavorable for its applications. Therefore, the simultaneous achievement of both high efficiency and broad bandwidth for a metalens should carefully consider both phase manipulation for a given wavelength and phase error correction for the other wavelengths. In reality, it is quite challenging for phase manipulation to build the meta-atoms with proper structures and

configurations to realize broadband achromatic metalenses with high efficiencies. Recently, broadband achromatic metalenses were reported to be realized in the visible[20,22,25–27], infrared[28–31], or spanning the visible and near-infrared[31,32] successfully. However, both their efficiencies and bandwidths need to be enhanced, such as the only efficiency of 40% for a bandwidth of 260 nm from 400 to 660 nm[25] and maximum efficiency of 50% for a bandwidth of 450 nm from 1200 to 1650 nm[33]. Only more recently, a higher and broader bandwidth was achieved with an average efficiency of over 70% for a bandwidth of 550 nm from 650 to 1200 nm[31].

Here, we proposed an aperture-shared partition phase cooperative manipulation (APPCM) approach to design broadband achromatic metalenses with high focusing efficiency and a narrow range of FL change. The metalens is designed into two concentric sub-metalenses with inner circular and outer ring regions for different FLs, respectively. Both the phase profiles are combined to form a wavefront of the target metalens. The achromatic polarization-independent Si_3N_4 dielectric metalens with a diameter of $D = 46$ μm and a numerical aperture of NA = 0.107 is designed for the operation wavelengths spanning the visible and near-infrared. A bandwidth as broad as 950 nm ($\lambda = 450$–1400 nm) with near-constant FLs is realized with the focusing efficiencies over 70% for $\lambda = 600$–1400 nm.

2. Methods

2.1. Modified method for broadband achromatic metalens design

The phase profile of a metalens can be derived from Fermat's theorem[34], given as the following:

$$\varphi(\lambda,R,f) = -\frac{2\pi}{\lambda}\left(\sqrt{R^2+f^2}-f\right), \tag{1}$$

where λ is the wavelength of the incident light, R ($R = \sqrt{x^2+y^2}$) is the distance from an arbitrary position (x, y) on the metalens to the center (assuming the metalens is located in the plane of $z = 0$), and f is the FL of the metalens. It is obvious that f is a function of wavelength λ, which is an inherent property of the equation. However, for a broadband achromatic metalens, the FL is required to keep constant within the bandwidth of $[\lambda_{\min}, \lambda_{\max}]$. Substituting $\lambda_{\min}$ and $\lambda_{\max}$ into Eq. (1), we get a general condition of the phase profile of a broadband achromatic metalens:

$$2\pi\left(\sqrt{R^2+f^2}-f\right) = \frac{\varphi(\lambda_{\max},R,f)-\varphi(\lambda_{\min},R,f)}{\frac{1}{\lambda_{\max}}-\frac{1}{\lambda_{\min}}}, \tag{2}$$

$$\varphi(\lambda,R,f) = \frac{\varphi(\lambda_{\max},R,f)-\varphi(\lambda_{\min},R,f)}{\frac{1}{\lambda_{\max}}-\frac{1}{\lambda_{\min}}}\cdot\frac{1}{\lambda}. \tag{3}$$

According to Eqs. (2) and (3), the phase profiles at an arbitrary operation wavelength of λ can be determined for the predetermined FL and maximum/minimum wavelength $\lambda_{\min}/\lambda_{\max}$, which is linearly dependent on the wavenumber $1/\lambda$ with the slope determined by the phase profiles at the maximum and minimum wavelengths. When designing a meta-atom to manipulate the required phase at a given position R, the slope γ can be expressed using the phase imparted on the meta-atom, $\varphi(\lambda,S,E)$ at $\lambda_{\min}/\lambda_{\max}$, where λ is the wavelength of the incident light, S and E are structure parameter and boundary condition of the meta-atom:

$$\frac{\varphi(\lambda_{\max},S,E)-\varphi(\lambda_{\min},S,E)}{\frac{1}{\lambda_{\max}}-\frac{1}{\lambda_{\min}}} = \gamma = \frac{\varphi(\lambda_{\max},R,f)-\varphi(\lambda_{\min},R,f)}{\frac{1}{\lambda_{\max}}-\frac{1}{\lambda_{\min}}}. \tag{4}$$

Then, the phase at other wavelengths becomes

$$\varphi(\lambda,R,f) = \frac{\varphi(\lambda_{\max},S,E)-\varphi(\lambda_{\min},S,E)}{\frac{1}{\lambda_{\max}}-\frac{1}{\lambda_{\min}}}\cdot\frac{1}{\lambda} = \gamma\cdot\frac{1}{\lambda}, \tag{5}$$

revealing a linear wavenumber dependence of the imparted phase of the meta-atom required by a perfect achromatic metalens. Generally, the chromatic aberrations at other wavelengths are compensated using the slope γ. However, the real phase imparted on the meta-atom against the wavenumber is normally nonlinear due to the dispersion properties of the constituent material, which would induce the material-dependent intrinsic phase errors to cause the change of FL against the working wavelength. Moreover, a shift is inevitable for the imparted phase on each meta-atom because of the changes of the boundary condition for each meta-atom chosen from periodic during optimization to aperiodic. Thus, a phase shift $\Delta\varphi$ [$\varphi'(\lambda,S,E') = \varphi(\lambda,S,E) + \Delta\varphi$] could be reasonably introduced into the real phase of the meta-atom[35]. As a consequence, a non-negligible discrepancy is present between the real and target FLs, as shown in Fig. 1(a). The phase shifts would change the slope of phase versus wavenumber and thus may reduce the bandwidth, as revealed by the following formula:

$$\frac{\varphi(\lambda_{\max},S,E)-\varphi(\lambda_{\min},S,E)}{\frac{1}{\lambda_{\max}}-\frac{1}{\lambda_{\min}}} + \frac{\Delta\varphi_{\max}-\Delta\varphi_{\min}}{\frac{1}{\lambda_{\max}}-\frac{1}{\lambda_{\min}}} = \frac{\varphi(\lambda_{\max},R,f)-\varphi(\lambda_{\min},R,f)}{\frac{1}{\lambda_{\max}}-\frac{1}{\lambda_{\min}}}. \tag{6}$$

To address this issue, we proposed a strategy to reduce the influence of the phase shift that occurred in the general method above. We modify the method by focusing on the changes of the phase profile of the metalens composed of all meta-atoms instead of the phase shift of each meta-atom. The superposition principle of the wavefronts of light allows us to propose an APPCM approach of designing a broadband achromatic metalens, which is illustrated in Fig. 1(b). The designed metalens consists of two aperture-shared sub-metalenses Z1 and Z2. The meta-atoms in the inner circular Z1 and outer ring Z2 trim the phase profiles of f_1 and f_2, respectively. The combined phase profiles, along with the phase shift compensation effect from two

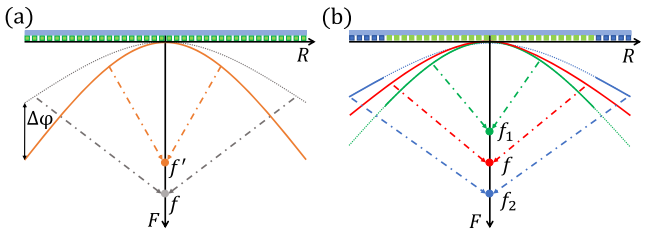

Fig. 1. Schematic diagram of the phase profiles of broadband achromatic metalenses. (a) The phase profile of a generally designed achromatic metalens. The gray dashed line is the theoretically calculated phase profile of focal length f. Due to the phase shift $\Delta\varphi$ of the selected meta-atoms determined using a periodic boundary condition, the actual phase profile of the metalens becomes a brown solid line, and the corresponding focal length changes to f'. For other wavelengths in the bandwidth range, the focal lengths have similar changes, so that the focal lengths in the entire bandwidth range are not exactly the same, and the purpose of the wide bandwidth cannot be achieved. (b) The phase profile of a broadband achromatic metalens using APPCM. For a certain wavelength λ, the green solid line is the phase profile with focal length f_1 designed in the Z1 zone (inner), the blue solid line is the phase profile with focal length f_2 designed in the Z2 zone (outer), and the red solid line is the overall phase profile corresponding to the focal length f, which is between f_1 and f_2. The combination of both phase profiles and the compensation of the phase shifts caused by both the zones make the overall focus lengths stay almost the same for all wavelengths within the bandwidth.

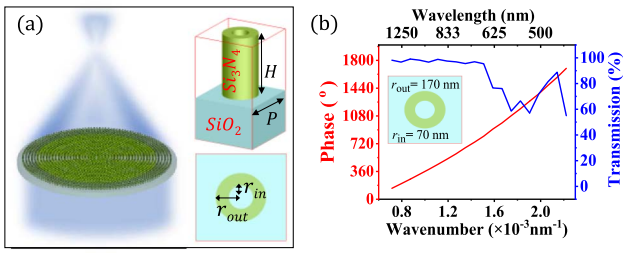

Fig. 2. (a) Schematic of an achromatic metalens composed of cylindrical Si_3N_4 ride meta-atoms. The height of the hollow nano-cylinder is 1500 nm, and the period of the meta-atoms (P) is 450 nm. (b) Wavenumber dependences of transmission (blue) and phase (red) for the meta-atom. The high transmission and a nearly linear phase as a function of the wavenumber are achieved in the entire visible region. The inset shows the geometry of the hollow nano-cylinders, where the outer and inner radii of the ring are 170 nm and 70 nm, respectively.

regions, account for the resultant phase profile of the target FL. The FL, f, of the metalens designed using APPCM can be easily derived to be between f_1 and f_2.

Diffraction theory is utilized to decide the position of the focal point. When a plane wave irradiates on two sub-metalenses, the output intensity I_z along the optical axis can be approximated as[13]

$$I_z = \sum_{i=1}^{n} N_i \cdot I_i, \qquad 1 \le i \le n, \tag{7}$$

where i is the ordinal number of the metalens rings from inside to outside, n is the total number of rings, N_i is the total number of meta-atoms corresponding to i, and I_i is the interference intensity of the meta-atom corresponding to ring i at any position on the optical axis (Z axis). Monte Carlo simulations are performed with 100 simulations for the FLs of different wavelengths of Z1 and Z2 using a homemade code combined with Eq. (7)[32]. Results, presented in Section 4 of Supplementary Materials, indicate that the phase shift $\Delta\varphi$ of about 90° affects the position of the focal point and decreases the bandwidth of the metalens, but a reasonable allocation of Z1 and Z2 will help to reduce the adverse effect of the phase shift.

2.2. Design of the broadband achromatic metalens

As mentioned above, the entire metalens was designed into two sub-metalenses, Z1 and Z2, using APPCM. The meta-atoms in Z1 and Z2 were optimized individually by using the general method and manipulating the phase profiles of the sub-metalenses with the FLs of f_1 and f_2, respectively. Nearly zero absorptive silicon nitride (Si_3N_4) at the visible and near-infrared wavelengths is taken as the meta-atom material on a quartz substrate to achieve high focusing efficiency[36] (see Supplementary Materials, Fig. S1). Nano-cylinders with high symmetry and contrast are used as the basic structures of meta-atoms to improve the focusing efficiency and realize polarization independence as well[22,33], as shown in Fig. 2(a). The height and the lattice constant of the meta-atoms were set as 1500 nm and 450 nm, respectively. Both the inner and outer radii of nano-cylinders were optimized within the range of 15–200 nm, and a group of nano-cylinders with high transmission was collected for a meta-atom library.

The wavenumber dependences of the phase and transmittance of nano-cylinders were obtained by simulation using the finite-difference time-domain (FDTD) method[37] (see Appendix A for details). Figure 2(b) shows the transmission and phase spectra of a nanocylinder with the outer and inner radii of 170 nm and 70 nm, respectively, under the normal incidence of x-polarized light. It can be seen that the phase in the Fig. 2(b) increases almost linearly with the wavenumber in the full spectral region, which is a prerequisite for designing a broad bandwidth achromatic metalens. Figure 2(b) also shows very high and steady transmission (blue line) close to 100% for the wavelengths larger than 680 nm and then the transmission tends to drop still with a high level over 60% upon getting closer to the lattice constant. The gradually decreased transmittance from 450 to 680 nm is believed to be a result of high-order diffractions.

To verify the concept of above APPCM, we designed a broadband achromatic metalens (M1) with a 950 nm bandwidth in the wavelength range of 450–1400 nm using the hollow nano-cylinder Si_3N_4 meta-atoms. The FLs of Z1 and Z2 are 200 μm and 250 μm, respectively. To optimize the accuracy of phase manipulation of the chosen nano-cylinders, many more nano-cylinders are simulated with the phases imparted for the maximum (1400 nm) and minimum (450 nm) wavelengths, as shown in Fig. 3(a) (light blue dots). The required phases of Z1 and Z2 at the maximum and minimum wavelengths are

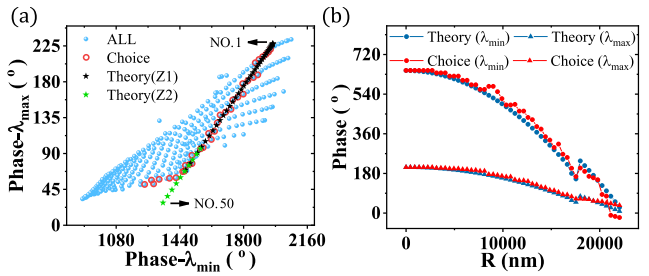

Fig. 3. (a) Simulation of the phase manipulation of Si_3N_4 nano-cylinders. The light blue solid dots represent the phases imparted on the nano-cylinders with different inner and outer radii at the maximum and minimum wavelengths. The black and green stars are the theoretically calculated phases for the Z1 zone (f_1 = 200 μm) and the Z2 zone (f_2 = 250 μm), respectively. It should be noted that some black stars and green stars overlap due to different diameters and FLs for Z1 and Z2. The first black star on the upper right and the last green star on the lower left represent the first unit and the last unit, respectively. All units are arranged in order from top to bottom to be matched. (b) Phase profiles of the broadband achromatic metalens M1 designed using the APPCM approach. The phase manipulation using the chosen nano-cylinders (red) is basically following the theoretical calculations (blue).

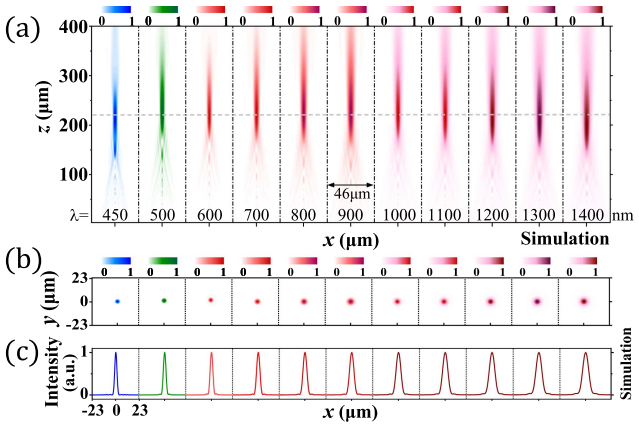

Fig. 4. Normalized intensity distribution of the broadband achromatic metalens M1. (a) Simulated normalized intensity profiles in the plane $x = 0$ (y–z plane) around the focal point of metalens M1 at different wavelengths. The gray dashed line is the average (214 μm) of the focal lengths for all wavelengths. (b) Intensity profiles in the focal plane (x–y plane) of M1 at different wavelengths. (c) Longitudinal cross sections of the corresponding focal spots in (b).

shown using black and green stars, respectively. The phases imparted on the chosen nano-cylinders are selected close to the phases required by two zones as much as possible, as indicated by those red circles. One should bear in mind that the numbers of meta-atoms in both zones are almost equal for the achievement of maximum bandwidth in this design, because the number of meta-atoms contributing to each phase value increases with the increasing of radius R. The phase profiles of the inner circle and outer ring form a new phase profile corresponding to FLs. (The statistical results in Section 4 of Supplementary Materials show that the bandwidth will be stabilized within 5% in the case of Z1:Z2 ≈ 40:10.)

The phase profiles of the metalens (M1) composed of the chosen nano-cylinders versus the radius of the metalens are shown in Fig. 3(b). The phases in both zones can be found to be basically consistent with the corresponding theoretical calculations. It should be noted that the simulated phase of the selected structural unit is different from the phase of our theoretical design. We have theoretically proved that a common amount of phase shift is completely equivalent (see Section 3 of Supplementary Materials).

3. Results and Discussion

The performance of the broadband achromatic metalens designed using the APPCM approach was simulated under the illumination of a normally incident x-polarized plane wave onto the metalens from the quartz substrate[38]. Figure 4(a) shows the normalized intensity profiles of the metalens M1 in the plane $x = 0$ (y–z plane) at different wavelengths. The plane waves for different wavelengths in the range of 450–1400 nm were focused at almost the same position ($Z = 214$ μm), suggesting the achromatic metalens with a 950 nm bandwidth spanning the visible and near-infrared, as designed. The intensity profiles of M1 in the focal plane (x–y plane) for different wavelengths and their corresponding longitudinal cross sections of focal spots are shown in Figs. 4(b) and 4(c), respectively. The results show nearly diffraction-limited focusing for all wavelengths with no obvious distortion.

It is worth noting that the FL of a broadband achromatic metalens usually varies at different wavelengths due to the errors between the phase manipulation by the meta-atoms and the theoretical one. To better evaluate the discrepancies of FLs at different wavelengths, we introduced the concept of the coefficient of variation (CV) in statistics[39]:

$$\mathrm{CV} = \frac{\mathrm{SD}}{\mathrm{MN}} \times 100\%, \tag{8}$$

where $\mathrm{MN} = \frac{1}{n}\sum_{i=1}^{n} f_i$ is the average, and $\mathrm{SD} = \sqrt{\frac{1}{n}\sum_{i=1}^{n}(f_i - \mathrm{MN})^2}$ is the standard deviation.

Here, CV for M1 is derived to be 4.05%, which is within the allowed scope (5%) of the international standard of chromatic aberration. To demonstrate that an achromatic metalens designed using the APPCM approach can improve the FL variation, we took the sub-metalens Z1 as an individual metalens with FL of 200 μm for comparison. The deviation of FLs for Z1 is shown in Fig. 5(a) (gray round-dot-line) and Supplementary Materials, Fig. S7(a). The maximum discrepancy reaches as large as 80 μm with CV = 14.79%. Furthermore, another metalens M1' with the same size and focal length as M1 was designed, and its CV is 11.7% [see Supplementary Materials, Fig. S7(d) for normalized intensity distribution]. These results show that the APPCM method can effectively suppress FL fluctuations. To assess the capability of the APPCM approach suppressing

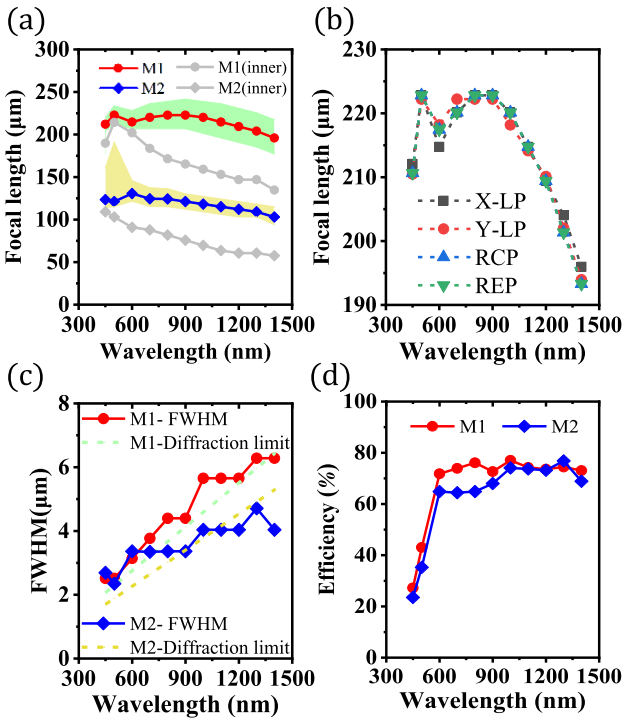

Fig. 5. Performances of broadband achromatic metalenses M1 and M2. (a) Focal length as a function of wavelength for metalenses M1 and M2. The round-dot line and the diamond-dot line represent the focal lengths of M1 and M2, respectively. The red and blue lines are the focal lengths of the entire metalens, whereas the gray line is the focal length of the inner zone. The green and yellow shadow areas demonstrate the DOF of M1 and M2 at different wavelengths, respectively. (b) Simulated focal lengths of M1 for *X*, *Y* polarizations (*X*-LP, *Y*-LP), right-handed circular polarization (RCP), and right-handed elliptical polarization (REP). (c) Simulated FWHMs at different wavelengths. The red round and blue diamond dots are the FWHMs of M1 and M2, respectively. The green and yellow dotted lines represent the theoretical FWHMs of metalenses M1 and M2. (d) The red round and blue diamond dots give the wavelength dependence of the focusing efficiency of metalenses M1 and M2, respectively.

the FL fluctuation of a metalens, we designed another metalens M2 (NA = 0.132) with the same bandwidth but a different FL from M1. The focusing of M2 for different wavelengths is shown in Fig. 5(a) (diamond-dot-line) and Supplementary Materials, Figs. S7(b) and S7(c). The discrepancies of the FLs for different wavelengths were also reduced as expected (CV = 4.83%). Besides the FL, the depth of focus (DOF) is another important parameter for a lens, which is defined as the range around the focus with the normalized intensity over 0.95[22]. The DOFs of M1 and M2 for different wavelengths are shown with green and yellow areas in Fig. 5(a), respectively.

The nano-cylinder-based metalenses are intuitively expected to be polarization-independent[22,33]. To prove this point, simulations were performed on the focusing of M1 with the illuminations of four different polarizations, i.e., *X*, *Y* polarizations (*X*-LP, *Y*-LP), right-handed circular polarization (RCP), and right-handed elliptical polarization (REP). The simulated results shown in Fig. 5(b) reveal almost the same FLs at different wavelengths for different polarizations.

Diffraction-limited focal spots of lenses are recognized to be capable of improving the imaging resolution, which is a key performance parameter for imaging systems[33]. The full width at half-maximum (FWHM) of a focal spot can be adopted to estimate the imaging resolution, and thus the FWHMs of the focal spots of M1 and M2 for different wavelengths are shown in Fig. 5(c). The FWHMs for different wavelengths are close to their theoretical limits (0.5/NA), demonstrating the near-diffraction-limited focusing capability of the designed metalenses in the full bandwidth. Also, another crucial performance parameter for a metalens was the focusing efficiency, which is defined as the ratio of total electric field intensity within the range of three times the FWHM of the focal spot to the total electric field intensity of incident light[38]. The focusing efficiency of M1 is over 70% within the wavelength range from 600 nm to 1400 nm, as shown in Fig. 5(d). High-order diffractions resulted in the rapidly decreased efficiency as the wavelength gets closer to the lattice constant of meta-atoms, i.e., from 450 nm to 600 nm. The inset in Fig. 5(d) presents the efficiency of M2 over 60% with the wavelength ranging from 600 nm to 1400 nm. (Compared with the reported broadband achromatic metalenses, whose focusing efficiencies have fluctuated at the working wavelength[22,25], the achromatic metalenses we designed demonstrate the efficiencies in a high level at different wavelengths, which provides the possibility for application of high-efficiency metalenses with broad bandwidth.)

4. Conclusion

Accurate phase manipulation for a metalens based on metasurfaces is normally indispensable for the realization of powerful functionalities with superior performances, but it is quite challenging. We thus proposed the APPCM approach, which makes it possible to design high-performance metalenses in terms of the effects of phase shift compensation and phase error correction for different wavelengths. The distortion of phase shifts would possibly lead to the fluctuation of focal length with the wavelength, the degradation of focusing efficiency, and the bandwidth narrowing of a metalens. We successfully demonstrated the feasibility of the APPCM approach by designing the high-performance metalens with the hollow nano-cylindrical Si_3N_4 dielectric meta-atoms on a quartz substrate. The metalens was designed into two sub-metalenses composed of the meta-atoms with different configurations optimized to individually manipulate the phase profiles of different focal lengths using the conventional method. The combined phase profiles and the phase shift compensation of two sub-metalenses account for the resultant phase profile of the target focal length, which effectively suppresses the fluctuation of the focal lengths for different wavelengths to improve the stability of high focusing efficiency. The designed broadband achromatic polarization-independent metalens shows a bandwidth as broad as 950 nm ranging from 450 to 1400 nm, and the high focusing efficiencies

over 70% with a maximum of 77%. The CV of the focal lengths in the full bandwidth is only 4.05%. The metalens designed using the ACCPM approach presents outstanding performances compared to the literature from the perspectives of both bandwidth and focusing efficiency. The ACCPM approach provides a novel design platform for high-performance metalenses and other metasurfaces, which have potential for imaging in various fields such as self-driving vehicles, robotic vision, and virtual reality.

Appendix A: Numerical Simulation

All numerical simulations were carried out with the commercialized FDTD software (FDTD Solutions, Lumerical Inc.). For the simulation of unit elements, a unit cell with periodic boundary conditions and x-polarized normal incidence is employed for the simulation of transmission spectra and phase profile. For the simulation of a metalens, a perfectly matched layer (PML) is employed as the boundary condition for the x and y directions to mimic a free space for far-field scattering simulation. To block injection of the field beyond the lens, an aperture made of perfect electric conductor (PEC) material was placed right before the metalens.

Acknowledgement

The authors thank Shan Wu, Haifeng Hu, Taoran Xu, and Wentao Wang for helpful discussions. This work was supported by the National Natural Science Foundation of China (Nos. 61875042, 11627803, DMR-61804010, and 11204209), Youth Innovation Promotion Association CAS (No. Y201911), Scientific Instrument Developing Project CAS (No. Y8512911), and Natural Science Foundation of Tianjin (No. 17JCYBJC16200).

References

1. Q. T. Li, F. Dong, B. Wang, F. Gan, J. Chen, Z. Song, L. Xu, W. Chu, Y. F. Xiao, Q. Gong, and Y. Li, "Polarization-independent and high-efficiency dielectric metasurfaces for visible light," Opt. Express **24**, 16309 (2016).
2. A. Arbabi, E. Arbabi, Y. Horie, S. M. Kamali, and A. Faraon, "Planar metasurface retroreflector," Nat. Photon. **11**, 415 (2017).
3. Y. Zhou, I. I. Kravchenko, H. Wang, H. Zheng, G. Gu, and J. Valentine, "Multifunctional metaoptics based on bilayer metasurfaces," Light Sci. Appl. **8**, 80 (2019).
4. S. Wu, Z. Zhang, Y. Zhang, K. Zhang, L. Zhou, X. Zhang, and Y. Zhu, "Enhanced rotation of the polarization of a light beam transmitted through a silver film with an array of perforated S-shaped holes," Phys. Rev. Lett. **110**, 207401 (2013).
5. Z. Xuan, J. Li, Q. Liu, F. Yi, S. Wang, and W. Lu, "Artificial structural colors and applications," Innovation **2**, 100081 (2021).
6. M. Deng, T. Ren, J. Wang, and L. Chen, "Doublet achromatic metalens for broadband optical retroreflector," Chin. Opt. Lett. **19**, 071701 (2021).
7. A. Pors, M. G. Nielsen, R. L. Eriksen, and S. I. Bozhevolnyi, "Broadband focusing flat mirrors based on plasmonic gradient metasurfaces," Nano Lett. **13**, 829 (2013).
8. H. Yang, G. Li, X. Su, G. Cao, Z. Zhao, X. Chen, and W. Lu, "Reflective metalens with sub-diffraction-limited and multifunctional focusing," Sci. Rep. **7**, 12632 (2017).
9. M. Khorasaninejad and F. Capasso, "Metalenses: versatile multifunctional photonic components," Science **358** (2017).
10. Z. Li, C. Cheng, H. Liu, D. Li, S. Xu, H. Liu, J. Zhang, and S. Zhang, "Experimental generation of Kagome lattices using metasurface of integrated convex lens," Chin. Opt. Lett. **18**, 012201 (2020).
11. C. Jin, J. Zhang, and C. Guo, "Metasurface integrated with double-helix point spread function and metalens for three-dimensional imaging," Nanophotonics **8**, 451 (2019).
12. W.-L. Guo, G.-M. Wang, K. Chen, H.-P. Li, Y.-Q. Zhuang, H.-X. Xu, and Y. Feng, "Broadband polarization-conversion metasurface for a cassegrain antenna with high polarization purity," Phys. Rev. Appl. **12**, 014009 (2019).
13. W. Wang, Z. Guo, K. Zhou, L. Ran, Y. Sun, F. Shen, G. Fan, Y. Li, S. Qu, and S. Liu, "Metalens focusing the co-/cross-polarized lights in longitudinal direction," Plasmonics **12**, 69 (2016).
14. D. Tang, C. Wang, Z. Zhao, Y. Wang, M. Pu, X. Li, P. Gao, and X. Luo, "Ultrabroadband superoscillatory lens composed by plasmonic metasurfaces for subdiffraction light focusing," Laser Photon. Rev. **9**, 713 (2015).
15. Y. Bao, Q. Jiang, Y. Kang, X. Zhu, and Z. Fang, "Enhanced optical performance of multifocal metalens with conic shapes," Light Sci. Appl. **6**, e17071 (2017).
16. C. Williams, Y. Montelongo, and T. D. Wilkinson, "Plasmonic metalens for narrowband dual-focus imaging," Adv. Opt. Mater. **5**, 1700811 (2017).
17. Y. Yao and W. Wu, "All-dielectric heterogeneous metasurface as an efficient ultra-broadband reflector," Adv. Opt. Mater. **5**, 1700090 (2017).
18. M. Khorasaninejad, Z. Shi, A. Y. Zhu, W. T. Chen, V. Sanjeev, A. Zaidi, and F. Capasso, "Achromatic metalens over 60 nm bandwidth in the visible and metalens with reverse chromatic dispersion," Nano Lett. **17**, 1819 (2017).
19. X. Zhang, C. Guan, K. Wang, L. Cheng, J. Yang, J. Shi, H. Liu, Z. Liu, and L. Yuan, "Multi-focus optical fiber lens based on all-dielectric metasurface," Chin. Opt. Lett. **19**, 050601 (2021).
20. R. J. Lin, V.-C. Su, S. Wang, M. K. Chen, T. L. Chung, Y. H. Chen, H. Y. Kuo, J.-W. Chen, J. Chen, Y.-T. Huang, J.-H. Wang, C. H. Chu, P. C. Wu, T. Li, Z. Wang, S. Zhu, and D. P. Tsai, "Achromatic metalens array for full-colour light-field imaging," Nat. Nanotechnol. **14**, 227 (2019).
21. H. Pahlevaninezhad, M. Khorasaninejad, Y. W. Huang, Z. Shi, L. P. Hariri, D. C. Adams, V. Ding, A. Zhu, C. W. Qiu, F. Capasso, and M. J. Suter, "Nano-optic endoscope for high-resolution optical coherence tomography *in vivo*," Nat. Photon. **12**, 540 (2018).
22. Z.-B. Fan, H.-Y. Qiu, H.-L. Zhang, X.-N. Pang, L.-D. Zhou, L. Liu, H. Ren, Q.-H. Wang, and J.-W. Dong, "A broadband achromatic metalens array for integral imaging in the visible," Light Sci. Appl. **8**, 67 (2019).
23. M. Khorasaninejad, A. Y. Zhu, C. Roques-Carmes, W. T. Chen, J. Oh, I. Mishra, R. C. Devlin, and F. Capasso, "Polarization-insensitive metalenses at visible wavelengths," Nano Lett. **16**, 7229 (2016).
24. A. Arbabi, Y. Horie, A. J. Ball, M. Bagheri, and A. Faraon, "Subwavelength-thick lenses with high numerical apertures and large efficiency based on high-contrast transmit arrays," Nat. Commun. **6**, 7069 (2015).
25. S. Wang, P. C. Wu, V. C. Su, Y. C. Lai, M. K. Chen, H. Y. Kuo, B. H. Chen, Y. H. Chen, T. T. Huang, J. H. Wang, R. M. Lin, C. H. Kuan, T. Li, Z. Wang, S. Zhu, and D. P. Tsai, "A broadband achromatic metalens in the visible," Nat. Nanotechnol. **13**, 227 (2018).
26. W. T. Chen, A. Y. Zhu, V. Sanjeev, M. Khorasaninejad, Z. Shi, E. Lee, and F. Capasso, "A broadband achromatic metalens for focusing and imaging in the visible," Nat. Nanotechnol. **13**, 220 (2018).
27. W. T. Chen, A. Y. Zhu, J. Sisler, Z. Bharwani, and F. Capasso, "A broadband achromatic polarization-insensitive metalens consisting of anisotropic nanostructures," Nat. Commun. **10**, 355 (2019).
28. H. P. Zhou, L. Chen, F. Shen, K. Guo, and Z. Y. Guo, "Broadband achromatic metalens in the midinfrared range," Phys. Rev. Appl. **11**, 024066 (2019).
29. S. Wang, P. C. Wu, V. C. Su, Y. C. Lai, C. Hung Chu, J. W. Chen, S. H. Lu, J. Chen, B. Xu, C. H. Kuan, T. Li, S. Zhu, and D. P. Tsai, "Broadband achromatic optical metasurface devices," Nat. Commun. **8**, 187 (2017).
30. B. Yu, J. Wen, X. Chen, and D. Zhang, "An achromatic metalens in the near-infrared region with an array based on a single nano-rod unit," Appl. Phys. Express **12**, 092003 (2019).
31. F. Balli, M. Sultan, S. K. Lami, and J. T. Hastings, "A hybrid achromatic metalens," Nat. Commun. **11**, 3892 (2020).

32. A. Ndao, L. Hsu, J. Ha, J. H. Park, C. Chang-Hasnain, and B. Kante, "Octave bandwidth photonic fishnet-achromatic-metalens," Nat. Commun. **11**, 3205 (2020).
33. S. Shrestha, A. C. Overvig, M. Lu, A. Stein, and N. Yu, "Broadband achromatic dielectric metalenses," Light Sci. Appl. **7**, 85 (2018).
34. N. Yu, P. Genevet, M. A. Kats, F. Aieta, J. P. Tetienne, F. Capasso, and Z. Gaburro, "Light propagation with phase discontinuities: generalized laws of reflection and refraction," Science **334**, 333 (2011).
35. L. Hsu, M. Dupre, A. Ndao, J. Yellowhair, and B. Kante, "Local phase method for designing and optimizing metasurface devices," Opt. Express **25**, 24974 (2017).
36. Z.-B. Fan, Z.-K. Shao, M.-Y. Xie, X.-N. Pang, W.-S. Ruan, F.-L. Zhao, Y.-J. Chen, S.-Y. Yu, and J.-W. Dong, "Silicon nitride metalenses for close-to-one numerical aperture and wide-angle visible imaging," Phys. Rev. Appl. **10**, 014005 (2018).
37. V. Liu and S. Fan, "S4: a free electromagnetic solver for layered periodic structures," Comput. Phys. Commun. **183**, 2233 (2012).
38. Z. P. Zhuang, R. Chen, Z. B. Fan, X. N. Pang, and J. W. Dong, "High focusing efficiency in subdiffraction focusing metalens," Nanophotonics **8**, 1279 (2019).
39. G. P. Rédei, "Coefficient of variation," in *Encyclopedia of Genetics, Genomics, Proteomics and Informatics*, G. P. Rédei, ed. (Springer Netherlands, 2008), p. 385.